Survival Analysis with Machine Learning for Predicting Li-ion Battery Remaining Useful Life

Jingyuan Xue[1,†] **Longfei Wei**[1,2,†] **Dongjing Jiang**[2,3] **Fang Sheng**[3,4]

Russell Greiner[5,6] **Jianfei Zhang**[1,2,3,*]

[1]ThinkX, Canada [2]DeepCox, China [3]MedicineX, Canada

[4]University of Toronto, Canada [5]University of Alberta, Canada [6]Amii, Canada

Abstract

Battery degradation significantly impacts the reliability and efficiency of energy storage systems, particularly in electric vehicles and industrial applications. Predicting the remaining useful life (RUL) of lithium-ion batteries is crucial for optimizing maintenance schedules, reducing costs, and improving safety. Traditional RUL prediction methods often struggle with nonlinear degradation patterns and uncertainty quantification. To address these challenges, we propose a hybrid survival analysis framework integrating survival data reconstruction, survival model learning, and survival probability estimation. Our approach transforms battery voltage time series into time-to-failure data using path signatures. The multiple Cox-based survival models and machine-learning-based methods, such as DeepHit and MTLR, are learned to predict battery failure-free probabilities over time. Experiments conducted on the Toyota battery and NASA battery datasets demonstrate the effectiveness of our approach, achieving high time-dependent AUC and concordance index (C-Index) while maintaining a low integrated Brier score. The data and source codes for this work are available to the public at https://github.com/thinkxca/rul.

1 Introduction

Battery aging and failure are inevitable processes that significantly impact the reliability and efficiency of energy storage systems, particularly in industrial applications and electric vehicles (EVs). As the core energy source in EVs, lithium-ion (Li-ion) batteries degrade over time due to complex chemical and physical interactions, leading to performance decline, reduced lifespan, and increased failure risk. This deterioration can result in higher maintenance costs, unplanned downtimes, and safety concerns. Hence, accurately predicting battery failure is essential for ensuring operational efficiency, minimizing costs, and improving safety (Lillelund et al., 2025).

[†]These authors contributed equally

[*]Corresponding author: zhang@thinkx.ca

One approach to understanding battery degradation is the remaining useful life (RUL) prediction, which estimates the remaining cycles or time before a battery reaches a critical failure threshold (typically 70-80% of its initial capacity). Effective RUL prediction allows for proactive maintenance, extending battery lifespan, optimizing maintenance schedules, and reducing overall lifecycle costs. However, accurately predicting RUL is challenging due to the highly stochastic nature of battery degradation, influenced by temperature, charge and discharge rates, and depth of discharge. Traditional RUL prediction methods primarily rely on time-series analysis, regression models, and extrapolation techniques (Ahwiadi and Wang, 2025). While these prediction methods provide valuable insights, they often struggle with non-monotonic degradation trends, require extensive historical data, and assume linear degradation relationships, leading to inaccuracies or prediction bias (Lin et al., 2024). Furthermore, many RUL prediction models fail to incorporate uncertainty quantification, making them less reliable in real-world applications.

Survival analysis offers a promising alternative for RUL prediction by modeling the failure as a probabilistic event over time rather than predicting a single failure point (Zhang et al., 2020). This approach leverages survival functions and hazard rates to estimate failure probabilities dynamically, allowing for real-time adjustments based on evolving battery health indicators. By utilizing survival probability predictions, users can select batteries that meet their longevity requirements, optimizing performance and cost-effectiveness. For example, the probability of a failure-free battery in a 5-year-old vehicle up to 1000 cycles is 90%, but for up to 2000 cycles the probability drops to 20%. Survival models, such as Cox Proportional-Hazards regression model (Cox, 1975), Kaplan-Meier estimators (Ragab et al., 2016), and Weibull distributions (Deng et al., 2023), have been widely used to characterize battery degradation processes. This motivates us to apply survival analysis to estimate the failure-free probability over time, rather than to forecast RUL directly.

A critical challenge in survival-analysis-based RUL prediction is handling censored data where the failure event has not yet been observed (Chen et al., 2020), where ignoring censored data can lead to biased time-to-failure estimates. To address this, recent research has incorporated high-dimensional feature extraction techniques, such as path signatures (Chevyrev and Kormilitzin, 2025), to capture high-order interactions and temporal dependencies in battery health indicators. By embedding battery voltage trajectory signatures, each battery sample can be associated with both time-to-failure data (number of cycles or time until failure) and censorship status (whether the battery has failed or remains operational at the last observation point). Hence, we will perform such data transformation so that we can learn powerful survival models from the transferred data.

Another critical challenge is that traditional survival models often impose restrictive assumptions *(e.g.*, the proportional hazards in the Cox model), limiting their adaptability to real-world battery aging scenarios. Additionally, they struggle to capture complex, nonlinear degradation patterns (Reza et al., 2024). A promising approach is to integrate machine learning methods into survival models, relaxing these assumptions and uncovering degradation patterns, which could enhance accuracy, reliability, and adaptability in RUL prediction.

Building on the above, we propose a novel survival analysis framework that integrates both traditional and machine-learning-based survival models for Li-ion battery RUL prediction. First, we employ the signature method to transform the time series of charging and discharging voltage into

time-to-failure data, making survival analysis models applicable. We then utilize five models, including statistical approaches – *e.g.*, Cox Cox (1975) and its revised models (Kvamme et al., 2019; Katzman et al., 2018), and machine-learning-based models – *e.g.*, DeepHit Lee et al. (2018) and MTLR (Yu et al., 2011), to predict the RUL by estimating the failure-free probabilities of batteries over time. Experiments conducted on two battery datasets (originally provided by Toyota and NASA) demonstrate that the survival models we learned from these data can accurately predict batteries' RUL, achieving high time-dependent AUC and concordance index (C-Index) while maintaining a low integrated Brier score (IBS) in time-to-failure prediction. The main contributions of this work are as follows:

- We propose a hybrid framework that integrates model-based and data-driven approaches for RUL prediction, evaluated on two real-world battery datasets from Toyota and NASA.
- We design a complete pipeline that transforms time-series data into time-to-failure formats, trains various survival models, and evaluates models' performance in terms of three survival metrics.
- We conduct comparative experiments and an ablation study, demonstrating the effectiveness and strong generalization capability of the proposed approach.
- We release all data and source code to facilitate reproducibility and extension to other battery RUL tasks, available at `https://github.com/thinkxca/rul`.

By leveraging survival analysis and machine learning, our methodology enhances the accuracy and robustness of RUL predictions, contributing to more efficient battery management systems and advancing predictive maintenance strategies for electric vehicles and industrial applications.

2 Related Work

RUL prediction methods are generally either model-based or data-driven (Hu et al., 2020). We will review recent work about these two approaches.

2.1 Model-based Approaches

Model-based approaches play a crucial role in battery health monitoring and RUL prediction by simulating battery behavior using physical, electrochemical, or equivalent circuit models (Ahwiadi and Wang, 2025). These models provide valuable insights into degradation mechanisms, operational impacts, and dynamic system behaviors (Li et al., 2014). By integrating theoretical principles with practical adaptability, model-based approaches enhance battery management system (BMS) performance and ensure long-term reliability. When combined with uncertainty quantification, these methods enable robust state estimation and RUL prediction under dynamic conditions (Kordestani et al., 2019). For instance, Mo et al. (2016) proposed integrating Kalman filtering and particle swarm optimization (PSO) into particle filters (PF) to refine RUL estimation, validated using the NASA battery dataset. Similarly, an extended Kalman particle filter (EKPF) (Duan et al., 2020) was developed to optimize PF sampling for improved accuracy. In (Al-Greer et al., 2023), a

physics-based prognostics framework was introduced by combining a single particle model (SPM) with a smooth particle filter (SPF), effectively capturing battery degradation mechanisms. Broadly speaking, model-based approaches adapt well to environmental changes, such as load fluctuations and temperature variations, enhancing their real-world applicability.

2.2 Data-driven Methods

Data-driven approaches leverage machine learning to directly learn nonlinear degradation behaviors from historical and real-time data (Li et al., 2024). Traditional methods include support vector regression (SVR), which offers high accuracy but is sensitive to parameter selection and lacks uncertainty quantification; relevance vector machine (RVM), which provides probabilistic outputs beneficial for reliability-critical applications but comes with higher computational costs; and Gaussian process regression (GPR), which models nonlinear relationships and provides confidence intervals but struggles with scalability issues (Liu and Chen, 2019; Xing et al., 2023). Recent advancements include (Xing et al., 2023), where principal component analysis (PCA) was applied to extract health indicators, and an improved Gaussian process regression (IGPR) was introduced for enhanced RUL prediction. Soft computing techniques further improve adaptability to complex degradation patterns. Artificial neural networks (ANNs) excel at capturing nonlinear relationships but require significant computational power and are prone to overfitting (Zhang et al., 2021). Adaptive neuro-fuzzy inference systems (ANFIS) integrate neural learning with fuzzy logic, enhancing interpretability and handling uncertainties, though performance heavily depends on initial rule selection. Zraibi et al. (2021) developed a hybrid model that combines an empirical battery model with a convolutional neural network (CNN) and long short-term memory (LSTM) network. This integration allows for accurate characterization of both the internal battery mechanisms and external environmental changes. Additionally, the beetle antennae search (BAS)-based particle filter (BAS-PF) was employed to compute battery parameters online. Compared to existing PF-based methods, BAS-PF effectively mitigates diversity loss and improves estimation accuracy. By integrating an electrochemical-thermal (ECT) model with an unscented Kalman filter (UKF), Ren et al. (2024) improved predictive performance even with incomplete or low-quality data. The ECT model captures the physics-based battery behavior, while the UKF iteratively updates parameters using machine learning, enhancing accuracy over time. Although these methods achieve accurate predictions, further improvements in feature extraction and hyperparameter tuning are needed to optimize battery management systems (Ahwiadi and Wang, 2025).

3 Our Method

In this section, we will present our feature extraction, time-to-failure data transformation, survival model training, and model evaluation methods.

3.1 Data Reconstruction

3.1.1 Feature Extraction

The charging and discharging voltages of electric vehicles and other battery-powered devices can be controlled in real-world applications, we thus consider the charging voltages as one of the features for extraction. In certain cases, consistent and controlled cycling conditions are required to study the intrinsic characteristics of batteries or battery-to-battery variations. Therefore, the discharging voltage is also included as a feature for extraction.

Given the voltage $V(t)$ at time t during the charging or discharging period, we represent the time-dependent voltage at the time $t \in [t_0, t_\infty]$ as a sequence $V(t) = (v_1(t), v_2(t), \ldots, v_M(t)) \in \mathbb{R}^M$. The k-depth truncated signature is a sequence of iterated integrals that capture the interactions along the sequence, *i.e.*,

$$S_k[V(t)] = \Big(\sigma_1[V(t)], \sigma_2[V(t)], \sigma_{1,1}[V(t)], \sigma_{1,2}[V(t)], \sigma_{2,1}[V(t)], \ldots, \sigma_{m_1,\ldots,m_k}[V(t)]\Big)$$
$$\sigma_k[V(t)] = \int_{t_0<t_k<t} \cdots \int_{t_0<t_1<t_2} dV^{(m_1)}(t_1) \cdots dV^{(m_k)}(t_k) \qquad m_1, \ldots, m_k \in \{1, 2, \ldots, M\}.$$

Here, $\sigma_k[V(t)]$ denotes the integrated integrals at depth k. The $\sigma_1[V(t)]$ represents the total elapsed time and the total voltage change, while other signatures capture pairwise interactions. For each battery's voltage curve, the feature is constructed as

$$\mathbf{x} = S_k[S_k[V(t)]] \in \mathbb{R}^{2(2^k-1)}, \tag{1}$$

which represents the time-varying voltage. By stacking the feature vectors of all N batteries, we obtain the feature matrix:

$$\mathbf{X} = (\mathbf{x}_1, \mathbf{x}_2, \ldots, \mathbf{x}_N) = \Big(S_k[S_k[V(t)]_1], S_k[S_k[V(t)]_2], \ldots, S_k[S_k[V(t)]_{m_1,\ldots,m_k}]\Big) \in \mathbb{R}^{N \times (2^{(k+1)}-2)}.$$

Concatenating the signatures across all batteries will build a high-dimensional data representation that effectively encodes temporal dependencies and non-linear interactions observed in the charging and discharging cycles. This approach effectively encodes the temporal and geometric features of the degradation process, enabling survival predictions despite variability in cycling conditions.

Note that the k-depth signature can balance model complexity, generalization, and computational cost, leading to more reliable and interpretable survival analysis results. Increasing the signature depth enhances the model's ability to capture complex interactions and higher-order dependencies. However, it also leads to an exponential growth in the dimensionality of the feature space, which can result in overfitting and increased computational cost. In this work, we choose $k = 3$ (which will be discussed in the experiment) to balance this trade-off by capturing sufficient non-linear interactions while maintaining a manageable feature dimension.

3.1.2 Time-to-Failure Formalization

The key to applying survival analysis is the transformation that transfers battery time-series into time-to-failure data. Time-series data typically consists of sequential observations, such as battery

voltage, capacity, and internal resistance, collected at regular intervals. In the context of battery RUL prediction, these time-series measurements provide valuable information about the degradation state of the battery over time. To convert this time-series data into time-to-failure data, we need to associate each battery's performance trajectory with the survival analysis framework.

In the survival analysis context, the 'event' refers to the occurrence of the battery's failure, which is defined when the battery's capacity falls below a predetermined threshold (e.g., 70-80% of its initial capacity). The 'time to failure' is the number of cycles or time until this failure occurs. Batteries that have not yet failed at the time of data collection are considered censored data. These batteries may continue to function, and their failure times are unknown. For these instances, time-to-failure data is represented by the last observed time point before the battery reaches the threshold or is removed from the dataset due to some other reason (e.g., maintenance, failure in testing). This transformation converts the time-series voltage data into a geometric trajectory that captures the temporal evolution of battery performance.

Denote by T a continuous non-negative random variable representing time to failure. Let the triplet $(\mathbf{x}, \tau, \zeta)$ express a battery, where its feature vector $\mathbf{x}$ is defined by Eq. 1. The censoring indicator outcome $\zeta = \mathbb{1}(T \leq C)$ equals 1 if battery capacity has dropped to 80% (or less) of its initial value and 0 otherwise. The scalar outcome time, τ, is either the minimum of time to failure, T, and or the (right-)censoring time, C, that is,

$$\tau = \min\{T, C\} = \begin{cases} T, & \text{if } \zeta = 1 \text{ (\textit{i.e.}, remaining capacity } \leq 80\%) \\ C, & \text{otherwise } \text{ (\textit{i.e.}, remaining capacity } > 80\%) \end{cases}$$

We shall assume without loss of generality that the individuals are ascendingly sorted according to observation, and T, C are conditionally independent given $\mathbf{x}$.

3.2 Model Learning

Usually, one adopts a survival probability $\Pr(T \geq t)$ to identify the probability of surviving (*i.e.*, still at risk of the failure event) by a prespecified time t. This probability is usually called survival probability or failure-free probability. The cumulative distribution function (CDF) of time-to-failure T is $F_c(t) = \Pr(T \leq t)$. The hazard rate $h(t)$ is the approximate probability of experiencing the event within a small time interval $\mathsf{d}t$, given that the individual has survived up to the beginning of the interval. That is, $h(t)$ assesses the instantaneous risk of a failure at time t, conditional on failure-free to t, given by

$$h(t) = \lim_{\mathsf{d}t \downarrow 0^+} \frac{\Pr(t \leq T \leq t + \mathsf{d}t \mid T \geq t)}{\mathsf{d}t}.$$

The numerator of this expression is the conditional probability that the event will occur in the interval $[t, t + \mathsf{d}t)$ given that it has not occurred before, and the denominator is the width of the time interval. It can be seen that the greater the value of $h(t)$, the greater the risk of failure at t. Furthermore, the cumulative (integrated) hazard function, $H(t)$, describes the probability of experiencing

the event in the period from time zero to t, *i.e.*,

$$H(t) = \int_0^t h(u)\mathrm{d}u.$$

In survival analysis, the hazard function fully determines the survival function, where we have

$$\Pr(T \geq t) = \exp(-H(t)).$$

Of note, the hazard function and survival function describe the instantaneous survival status and the cumulative survival status, respectively.

3.2.1 Cox-based Models

This study focuses on three Cox-type models, including the basic Cox, CoxTime, and CoxPH (which integrates into deep learning).

Cox Model The Cox model (Cox, 1975) is widely adopted and considers that the hazard is determined by prognostic variables in a multiplicative manner:

$$h(t \mid \mathbf{x}) = h_0(t)\exp(f_{\text{Cox}}(\mathbf{x}))$$
$$f_{\text{Cox}}(\mathbf{x}) = \boldsymbol{\beta}^\top \mathbf{x},$$

where $\boldsymbol{\beta} \in \mathbb{R}^{2(2^k-1)}$ is a vector of regression coefficients (*i.e.*, model parameters) describing how the hazard varies in response to the prognostic variables; $h_0(t)$ represents an arbitrary baseline hazard in the context of $\mathbf{x} = (0, \ldots, 0)^{2(2^k-1)}$, describing how the risk of event per time unit changes over time. For any two individual batteries $\mathbf{x}_1$ and $\mathbf{x}_2$, the hazard ratio is given by

$$\frac{h(t \mid \mathbf{x}_1)}{h(t \mid \mathbf{x}_2)} = \frac{h_0(t)\exp(\boldsymbol{\beta}^\top \mathbf{x}_1)}{h_0(t)\exp(\boldsymbol{\beta}^\top \mathbf{x}_2)} = \exp(\boldsymbol{\beta}^\top(\mathbf{x}_1 - \mathbf{x}_2)).$$

Since h_0 would be present in both the numerator and denominator, it cancels out and thus no assumption about the shape of the baseline hazard needs to be made; this yields an efficient computation, where the hazard ratio is independent of the baseline hazard function. This is why the Cox model is called hazards-proportional. The key to learning a Cox model lies in finding the value of $\boldsymbol{\beta}$ that maximizes the probability of the observed data, *i.e.*, maximize the likelihood of $\boldsymbol{\beta}$ given the observed data. As is generally the case, to estimate the likelihood we have to write the probability (or probability density) of the observed data as a function of $\boldsymbol{\beta}$. The Cox model aims to maximize the partial likelihood in the form:

$$L_{\text{Cox}} = \prod_{i \in \mathcal{Z}_1} \frac{\Pr\left(\text{battery failed at } T_i; \boldsymbol{\beta}\right)}{\Pr\left(\text{all batteries survive at } T_i; \boldsymbol{\beta}\right)} = \prod_{i \in \mathcal{Z}_1} \frac{\exp(\boldsymbol{\beta}^\top \mathbf{x}_i)}{\sum_{j \in \mathcal{R}(T_i)} \exp(\boldsymbol{\beta}^\top \mathbf{x}_j)},$$

where $\mathcal{Z}_1 = \{i : \zeta_i = 1\}$ is the set of all batteries that failed during the observation period.

CoxTime The proportionality assumption of the Cox model can be rather restrictive, and parameterizing the relative risk function with a neural net does not affect this constraint. A parametric approach, CoxTime (Kvamme et al., 2019), that does not require stratification and rebuilds a semi-parametric form of the Cox model, the relative risk function dependent on time is

$$h(t \mid \mathbf{x}) = h_0(t) \exp(f_{\text{CoxTime}}(\mathbf{x}))$$
$$f_{\text{CoxTime}}(t, \mathbf{x}_j) = a(t, \mathbf{x}) + b(t).$$

In this case, the hazards are no longer proportional. However, it is still a relative risk model with the same partial likelihood as previously. The loss function becomes

$$L_{\text{CoxTime}} = \frac{1}{|\mathcal{Z}_1|} \sum_{i \in \mathcal{Z}_1} \left(\sum_{j \in \mathcal{R}(T_i)} \exp\left(f_{\text{CoxTime}}(T_i, \mathbf{x}_j) - f_{\text{CoxTime}}(T_i, \mathbf{x}_i) \right) \right).$$

CoxPH CoxPH (also DeepSurv) (Katzman et al., 2018) is a deep feed-forward neural network that predicts the effects of features on their hazard rate parameterized by the weights of the neural network. The input to the network is a battery's features $\mathbf{x}$ defined in Eq. 1. The hidden layers of the network consist of a fully-connected layer of nodes, followed by a dropout layer. The output of the network $f_{\text{CoxPH}}(\mathbf{x}, \theta)$ is a single node with a linear activation that estimates the log-risk function in the Cox model. It trains the network by setting the objective function to be the average negative log partial likelihood with regularization:

$$L_{\text{CoxPH}} = \frac{1}{|\mathcal{Z}_1|} \sum_{i \in \mathcal{Z}_1} \left(\log \sum_{j \in \mathcal{R}(T_i)} \exp\left(f_{\text{CoxPH}}(\mathbf{x}_j, \theta) \right) - f_{\text{CoxPH}}(\mathbf{x}_i, \theta) \right).$$

3.2.2 Machine-Learning-based Models

Besides Cox-based models, we study two typical machine-learning-based survival models, i.e., DeepHit (Lee et al., 2018) and MTLR (Yu et al., 2011), which have been widely employed for most time-to-event prediction tasks.

DeepHit Model DeepHit (We consider its single-event version) (Lee et al., 2018) considers time to be discrete, so to fit it to the continuous-time data sets, we discretize the failure times with an equidistant grid between the smallest and largest duration in the training set. The number of discrete time-points is considered a hyperparameter. Assume time is discrete with $0, \ldots, \max\{T_i\}_{i=1}^N$, the survival probability for a single failure event is given by the subnets' output f, *i.e.*, $\Pr(T \leq t|\mathbf{x}) = f(t|\mathbf{x}; \mathbf{W})$. DeepHit optimizes a combination of likelihood loss and ranking loss to model survival times in a deep learning framework. The objective function is given by:

$$L_{\text{DeepHit}} = \alpha L_{\text{pmf}}(\mathbf{W}) + (1 - \alpha) L_{\text{rank}}(\mathbf{W})$$
$$L_{\text{pmf}}(\mathbf{W}) = -\sum_i \log(f(t|\mathbf{x}_i; \mathbf{W}))$$
$$L_{\text{rank}}(\mathbf{W}) = \sum_{i \in \mathcal{Z}_1, j} \zeta_i \cdot \mathbb{1}(T_i < T_j) \exp\left(\sigma\big(f(t|\mathbf{x}_i; \mathbf{W}) - f(T_i|\mathbf{x}_j; \mathbf{W}) \big) \right).$$

As described in the open-source implementation of (Lee et al., 2018), α represents the weighting factor between the likelihood loss and the rank loss, which differs from the model formulation stated in (Lee et al., 2018).

MTLR Multi-task learning regression (MTLR) * (Yu et al., 2011) performs multiple tasks simultaneously by sharing representations across tasks. In the context of battery RUL prediction, MTLR predicts the RUL for multiple batteries at once, learning shared features while predicting individual survival outcomes. For an batteries indexed as $i \in \mathcal{Z}_1 = \{i : \zeta_i = 1\}$, possessing known battery health statuses denoted as $Y = (y_1, \ldots, y_K)$ at times $t_1 < \cdots < t_K$, along with associated feature values $\mathbf{x}$ and regression coefficients $\Theta = (\boldsymbol{\theta}_1, \ldots, \boldsymbol{\theta}_K)$ where $\boldsymbol{\theta}_k$ serves to quantify the influence of features and their recurrent measurements on the probability of a battery's failure-free status, we estimate the probability of observing Y through the utilization of generalized logistic regression.

$$\Pr(Y|\mathbf{x};\Theta)_1 = \frac{\exp\left(\sum_{k=1}^{K} y_k \boldsymbol{\theta}_k \mathbf{x}\right)}{\sum_{k=0}^{K} \exp\left(\sum_{l=k+1}^{K} \boldsymbol{\theta}_k \mathbf{x}\right)}.$$

The numerator represents the accumulation of the risks associated with the occurrence of target responses. To learn the matrix Θ, we undertake minimization of the negative logarithm of the likelihood across all batteries through an expectation-maximization process. In MTLR, the objective is to minimize the loss function across multiple related tasks. This involves suitable initialization and can be outlined as follows:

$$L_{\text{MTLR}} = \lambda_1 \sum_{k=1}^{K} \|\boldsymbol{\theta}_k\|^2 + \lambda_2 \sum_{k=1}^{K-1} \|\boldsymbol{\theta}_{k+1} - \boldsymbol{\theta}_k\|^2 - \log L(\Theta)$$

$$L(\Theta) = \sum_{m=1}^{M} \left(\sum_{k=1}^{K} y_k(T_m) \boldsymbol{\theta}_k \mathbf{x}_m - \log \sum_{\kappa=0}^{K} \exp\left(\sum_{j=\kappa+1}^{K} \boldsymbol{\theta}_j \mathbf{x}_m\right) \right).$$

The regularization constants λ_1 for the first regularizer and λ_2 for the second regularizer control the amount of smoothing for the model and can be estimated via cross-validation.

4 Experiments

We implemented a robust experimental framework to evaluate the performance of survival models for predicting the RUL of Li-ion batteries.

4.1 Model Setting

All models were based on a multilayer perceptron (MLP) architecture, with optimized configurations: Cox, CoxTime, and CoxPH used two hidden layers (64 neurons per layer), Batch Normalization, and Dropout (0.1-0.2), with Adam optimizer (lr = 0.005), batch sizes of 128-256, and

*MTLR was originally developed by co-author Dr. Russell Greiner and his research team at the University of Alberta.

early stopping (patience=10). CoxTime discretized survival time into 10 intervals, while Cox and CoxPH computed risk via trapezoidal integration. DeepHit and MTLR followed similar architectures with discretized survival time, using 50 and 300 epochs, respectively, with interpolation-based risk computation. Optimizations included increased network capacity (64 neurons per layer), consistent dropout (0.1-0.2) for regularization, reduced learning rate (0.01 to 0.005) for stability, and Early Stopping adjustments, ensuring robust and comparable results across all models.

4.2 Dataset

The datasets, sourced from two battery manufacturers (Toyota and NASA), encompass diverse battery chemistries and charging conditions. Key data attributes include battery voltage, current, capacity, and internal resistance, collected over numerous charge-discharge cycles.

4.2.1 Toyota Data

The Toyota dataset originally comprises 373 Lithium Ferro Phosphate (LFP)/graphite A123 APR18650M1A cells. After removing 11 misclassified and noisy cells, 362 processed cells remained. For comparison, the cells were categorized into four groups, *i.e.*, G1: Batches 1-3 (129 cells), G2: Batches 4-5 (92 cells), G3: Batches 6-7 (96 cells), and G4: Batch 8 (45 cells). Each cell had an initial capacity of 1.1Ah and a voltage of 3.3V. Cycling tests were conducted under controlled conditions at 30°C. The discharge process followed a constant-current-constant-voltage (CC-CV) protocol at a 4C rate until the voltage dropped to 2.0V. Charging occurred in two stages: 1) from 0-80% state of charge (SOC) using one of 80+ charging policies, and 2) from 80-100% SOC with 1C CC-CV charge, reaching a maximum voltage of 3.6V.

Figure 1 (top) illustrates the voltage profile during charging. The charging curves show noticeable variations due to different charging strategies, highlighting their impact on the process. In contrast, despite identical cycling conditions, the discharging curves in Figure 1 (bottom) exhibit significant cell-to-cell differences, primarily attributed to the intrinsic properties of the cells. This indicates that even under the same cycling conditions, cell performance can vary. For each Toyota battery, voltage-time curves from the first 50 cycles were used as input, with separate signatures calculated for the charge and discharge phases.

The Toyota dataset includes two types of cells based on cycling termination. G1 (batches 1-3) and G4 (batch 8) were cycled until failure, defined as a remaining capacity of 80% of the initial value. In contrast, G2 (batches 4-5) and G3 (batches 6-7) were limited to 120 cycles, resulting in censored data. Figure 2 shows the end-of-life distribution, which ranges from 101 to 2235 cycles. Time-to-failure is determined from the capacity curves and is defined as the cycle number when the cell capacity decreases by 80% relative to its initial value. Significant differences in time-to-failure can be observed among different groups. For example, cells in groups G1 and G4 exhibit a wide range of cycle life distributions, while cells in groups G2 and G3 are all censored, with their time-to-failure truncated due to the termination of the experiment.

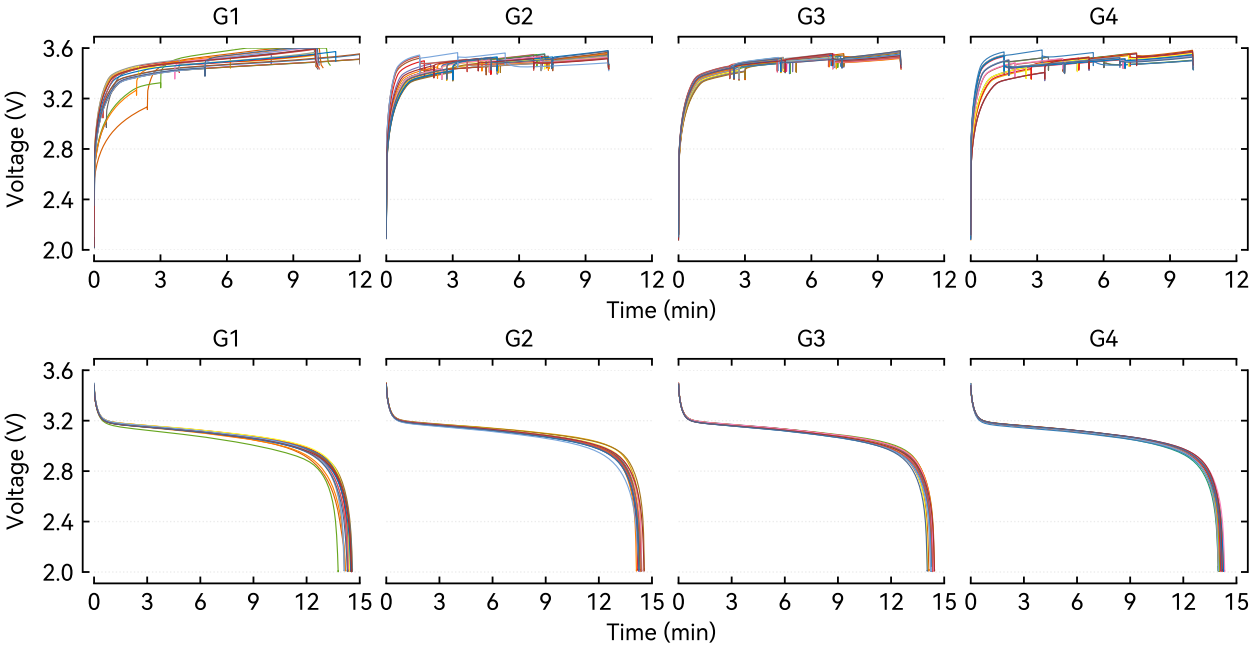

Figure 1: Toyota battery voltage change during charging (top) and discharging (bottom)

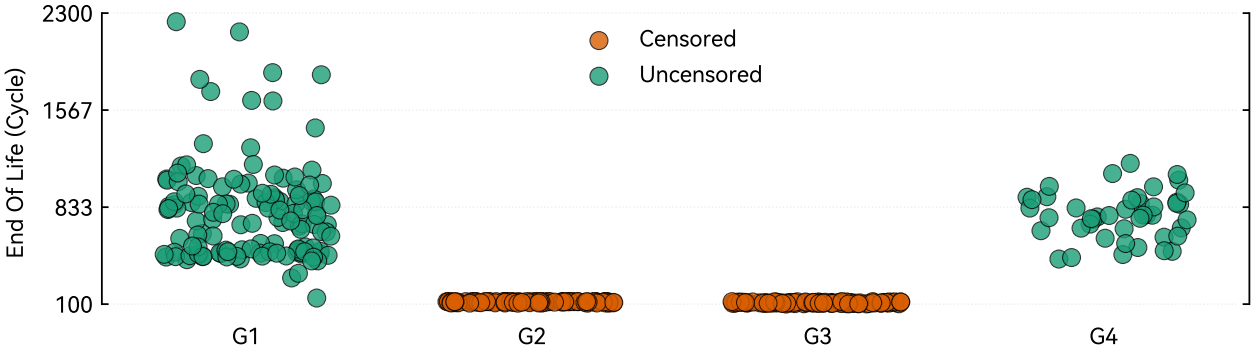

Figure 2: Time-to-failure status distribution across Toyota cell groups.

4.2.2 NASA Data

The NASA BatteryAgingARC-FY08Q4 dataset contains charge-discharge cycle data for lithium-ion batteries under constant operating conditions. For this study, we selected discharge data collected at 24°C with a constant current of 2A. Batteries 5, 6, 7, and 18 were analyzed, each using different voltage cutoffs (*e.g.*, 2.7V, 2.5V, 2.2V). Impedance measurements were performed via electrochemical impedance spectroscopy (EIS) over a frequency range of 0.1Hz to 5kHz. We treat each discharge cycle as an independent sample, collecting 636 samples (168 samples for batteries 5, 6, and 7, and 132 samples for battery 18). Their voltage change over time during the discharging process is plotted in Figure 3. A battery is considered failed if its capacity falls below 70% of the original (*i.e.*, 1.4Ah), corresponding to a discharge duration of approximately 2520 seconds. Battery failures total 44, 59, 0, and 36 for batteries 5, 6, 7, and 18, respectively. During preprocessing,

samples with an initial voltage of zero were removed, and records after discharge completion or beyond 2520 seconds were excluded.

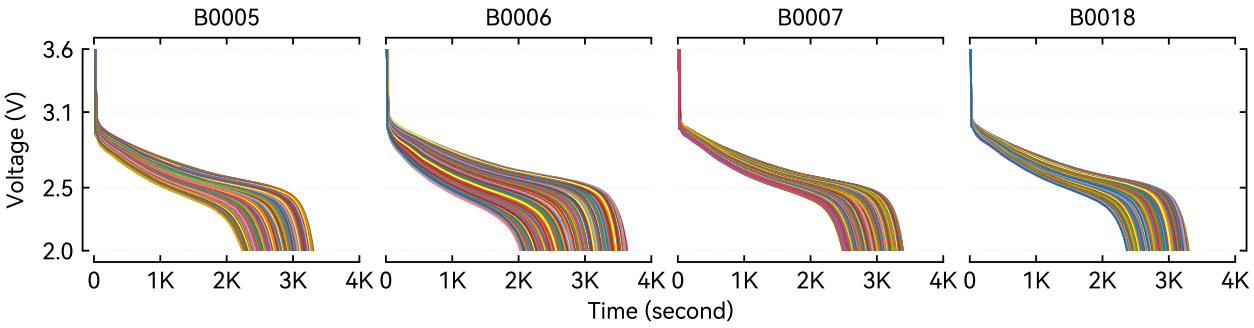

Figure 3: NASA battery voltage change during discharging

Figure 4 shows the survival distribution of battery samples. For B0005, B0006, and B0018, most batteries have been alive during the observation while a part failed (*i.e.*, voltage below 1.4). The end of life for all battery samples in terms of B0007 has been censored.

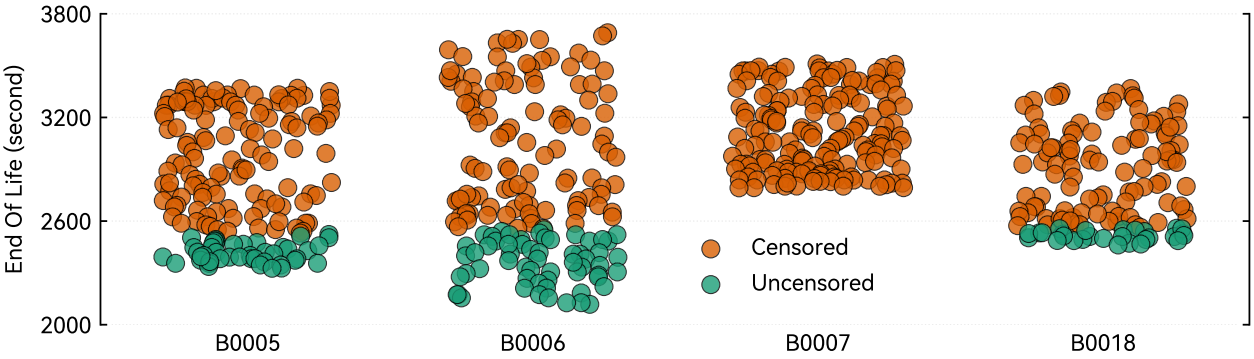

Figure 4: Time-to-failure status distribution across NASA battery groups.

4.3 Metrics

To maintain reproducibility, the dataset was uniformly stratified into training (80%), validation (5%), and test (15%) sets with a fixed random seed (random state=10). Performance on the test set of batteries was evaluated in terms of three independent metrics: the time-dependent AUC (T-AUC), the concordance index (C-Index), and the integrated Brier score (IBS), redefined as below:

- T-AUC provides a probability measure of classification ability over time. It quantifies the model's ability to address the issue *"Is battery i likely to remain alive by time t?"*.

$$\text{T-AUC} = \frac{1}{\max\{T_i\}_{i=1}^N} \int_0^{\max\{T_i\}_{i=1}^N} \frac{\sum_{i\in\mathcal{Z}_1}\sum_{j\in\mathcal{Z}_0} \mathbb{1}\{T_j > t\}\mathbb{1}\{T_i < t\} \frac{\mathbb{1}\{\Pr(\tau_i|\mathbf{x}_i)\le\Pr(\tau_i|\mathbf{x}_j)\}}{\text{KM}(t)}}{\left|\mathcal{Z}_0(t)\right| \times \sum_{i\in\mathcal{Z}_1(t)} \frac{\mathbb{1}\{T_i\le t\}}{\text{KM}(t)}} \mathsf{d}(\Pr(t))$$

$$\text{KM}(t) = \prod_{i:T_i<t} \left(1 - \frac{\sum_{j=1}^N \mathbb{1}\{T_j = T_i\}}{\sum_{j=1}^N \mathbb{1}\{T_j > T_i\}}\right).$$

  Here, $\mathcal{Z}_0(t) = \{i : T_i > t\}$ and $\mathcal{Z}_1(t) = \{i : T_i < t\}$. $\text{KM}(t)$ is the Kaplan-Meier estimate and $\frac{1}{\text{KM}(t)}$ is the inverse probability of censoring weights (IPCW).

- C-Index estimates how accurately the model can answer the question *"Which of battery i and battery j is more likely to remain alive?"*.

$$\text{C-Index} = \frac{1}{\left|\mathcal{Z}_1\right|} \sum_{i\in\mathcal{Z}_1} \frac{1}{\left|\{j : T_i < T_j\}\right|} \sum_{j:T_i<T_j} \mathbb{1}\{\Pr(T_i|\mathbf{x}_i) < \Pr(T_i|\mathbf{x}_j)\}.$$

- IBS measures an ensemble prediction error across the test data, i.e., the power of a model to address the question *"How accurate is the prediction that battery i will remain alive?"*. ($T_{\max}$ is the maximum of the time-to-failure in the test data; $\text{KM}(t)$ is the Kaplan-Meier estimate of the censoring failure-free probability at time t.)

$$\text{IBS} = \frac{1}{\max\{T_i\}_{i=1}^N} \int_0^{\max\{T_i\}_{i=1}^N} \frac{1}{\left|\mathcal{Z}_0\right| + \left|\mathcal{Z}_1\right|} \left(\sum_{i\in\mathcal{Z}_1} \frac{\Pr(t|\mathbf{x}_i)^2}{\text{KM}(T_i)} + \sum_{i\in\mathcal{Z}_0} \frac{(1-\Pr(t|\mathbf{x}_i))^2}{\text{KM}(t)}\right) \mathsf{d}t.$$

4.4 Results

4.4.1 Performance Comparison

Table 1 compares the five models' performance, in terms of T-AUC, C-Index, and IBS, on the charging and discharging data. The Cox model demonstrates strong performance across both phases, achieving the highest T-AUC in discharge (0.932) and a competitive C-Index (0.859), indicating excellent discriminative ability. CoxTime slightly outperforms Cox in the charge phase (T-AUC: 0.919 vs. 0.909), while maintaining a comparable IBS (0.028 vs. 0.031), suggesting better overall calibration. CoxPH, a simpler proportional hazards model, lags behind both Cox and CoxTime, particularly in T-AUC (0.889 in charge, 0.896 in discharge), indicating reduced predictive power. DeepHit, a deep learning-based survival model, exhibits mixed performance. While its C-Index is relatively strong (0.823 in charge, 0.816 in discharge), its T-AUC is significantly lower (0.730 in charge, 0.866 in discharge), suggesting challenges in capturing ranking information. Additionally, DeepHit's high IBS (0.085 in charge, 0.076 in discharge) indicates poor calibration, making its probability estimates less reliable. MTLR, a flexible survival model, balances performance between ranking and calibration, achieving a strong C-Index (0.844 in charge, 0.835 in discharge)

and relatively low IBS (0.040 in charge, 0.051 in discharge), making it a competitive alternative. Overall, Cox-based models (Cox, CoxTime, CoxPH) exhibit the most robust and consistent performance, particularly in T-AUC and IBS, reinforcing their effectiveness in survival analysis. DeepHit struggles with calibration despite its deep learning advantages, while MTLR provides a reasonable trade-off between discrimination and probability estimation. The results suggest that traditional survival models, particularly Cox and CoxTime, remain the most reliable choices for modeling charge and discharge survival patterns.

Table 1: Comparison of model performance on Toyota data

Model	Charge			Discharge		
	T-AUC	C-Index	IBS	T-AUC	C-Index	IBS
Cox	.909(.027)	.820(.030)	.031(.006)	.932(.018)	.859(.020)	.048(.008)
CoxTime	.919(.024)	.832(.033)	.028(.006)	.929(.018)	.853(.021)	.051(.009)
CoxPH	.889(.006)	.798(.015)	.035(.001)	.896(.037)	.826(.020)	.056(.012)
DeepHit	.730(.076)	.823(.044)	.085(.012)	.866(.059)	.816(.046)	.076(.020)
MTLR	.809(.058)	.844(.024)	.040(.007)	.922(.029)	.835(.025)	.051(.009)

Figure 5 presents the performance of five survival models on NASA discharge dataset. The CoxTime and CoxPH models achieve the best performance across all metrics, with near-perfect T-AUC (0.999), exceptionally high C-Index (0.998), and minimal IBS values (0.008 and 0.005, respectively), indicating accurate and well-calibrated RUL predictions. The Cox model also performs well (T-AUC: 0.993, C-Index: 0.946), though it trails slightly behind CoxTime and CoxPH, particularly in calibration (IBS: 0.036). MTLR delivers competitive results (T-AUC: 0.986, C-Index: 0.975), but its higher IBS (0.079) suggests slightly weaker calibration performance. In contrast, DeepHit shows significantly lower predictive accuracy (T-AUC: 0.872, C-Index: 0.757) and the highest IBS (0.185), indicating challenges in both discrimination and calibration for this dataset. This may be due to its sensitivity to the relatively limited sample size or the nature of the discharge patterns.

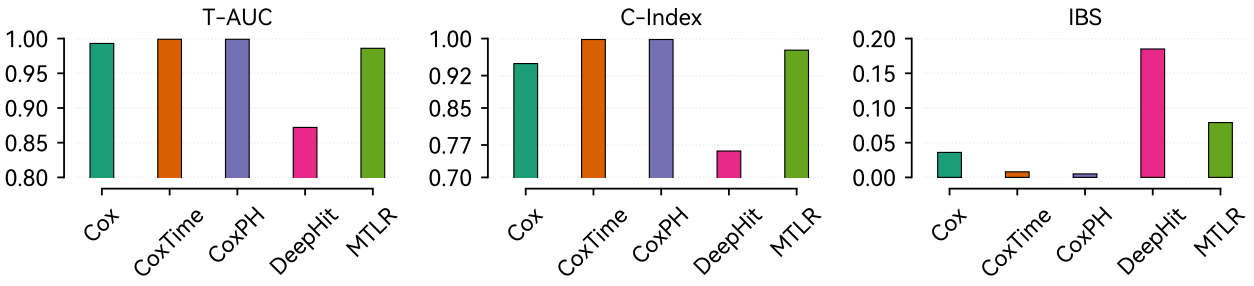

Figure 5: Comparison of model performance on NASA data

Figure 6 and Figure 7 show the estimated failure-free probability over time, for Toyota battery charging and discharging, respectively. Figure 8 gives the estimated failure-free probability over time, for NASA battery discharging. The Cox-based models generate smoother survival curves

that drop down quickly in a short period.. The three Cox-based models yield smoother curves, in comparison with DeepHit and MTLR. The main reason is the discrete time setting in DeepHit and MTLR. This is the same case for NASA battery discharging, as shown in Overall,

4.4.2 Ablation Study

We evaluated the predictive performance of the survival models using signature depths not only for $k = 3$ but also for $k = 2$ and $k = 4$. Figure 9 presents the change in C-Index when the models were performed on the data extracted from the original data using different signature depths. The comparative analysis of different survival models reveals distinct performance trends across the charging and discharging datasets. Generally, Cox and CoxTime models demonstrate strong predictive capabilities, particularly in the discharging dataset, where CoxTime achieves the highest C-Index (0.862) at signature depth 3. The Cox model consistently improves with increasing depth, showing robust performance, particularly in discharging (0.859 at depth 4), making it a competitive alternative to CoxTime. MTLR outperforms all models in the charging dataset, achieving the highest C-Index (0.851) at depth 3, indicating its effectiveness in handling the complexities of charge-related degradation patterns. DeepHit and CoxPH models show moderate performance, with CoxPH being the weakest performer due to its lower adaptability to nonlinear dependencies. Interestingly, while most models exhibit improved performance with increasing signature depth, some models (*e.g.*, CoxTime and DeepHit) show slight fluctuations, suggesting sensitivity to feature complexity. Results showed that $k = 3$ provided the best trade-off between model accuracy and computational efficiency, with diminishing returns observed for higher depths. Lower-order signatures (*e.g.*, $k = 2$) failed to capture the non-linear temporal patterns in the voltage curves, while higher-order signatures (*e.g.*, $k = 4$) led to overfitting, particularly in scenarios with limited training data. The choice of $k = 3$ ensures generalization and robustness across different battery groups and charging conditions.

Figure 10 shows the performance of the models when the sample fraction is changing from 25% to 100% (*i.e.*, training set equal to test set). The analysis of five survival models - Cox, CoxTime, CoxPH, DeepHit, and MTLR - demonstrates a consistent improvement in performance as the sample fraction increases from 0.25 to 1, highlighting the positive impact of larger datasets. Among them, MTLR emerges as the most stable and high-performing model across both charging and discharging data, showing steady and reliable gains with increasing sample size. CoxTime also stands out, exhibiting significant performance jumps, especially at higher sample fractions, making it one of the strongest models when more data is available. Cox and CoxPH, while reliable, do not exhibit as steep an improvement curve as CoxTime and MTLR, though they maintain competitive performance. DeepHit, in contrast, shows more variability, with some fluctuations in results across sample fractions, suggesting it may be more sensitive to data size changes. Overall, MTLR and CoxTime are the top-performing models for survival prediction, benefiting the most from increased data, while Cox and CoxPH remain solid choices with steady improvements. DeepHit, despite improving with larger sample fractions, demonstrates more instability, making it less favorable compared to the other models.

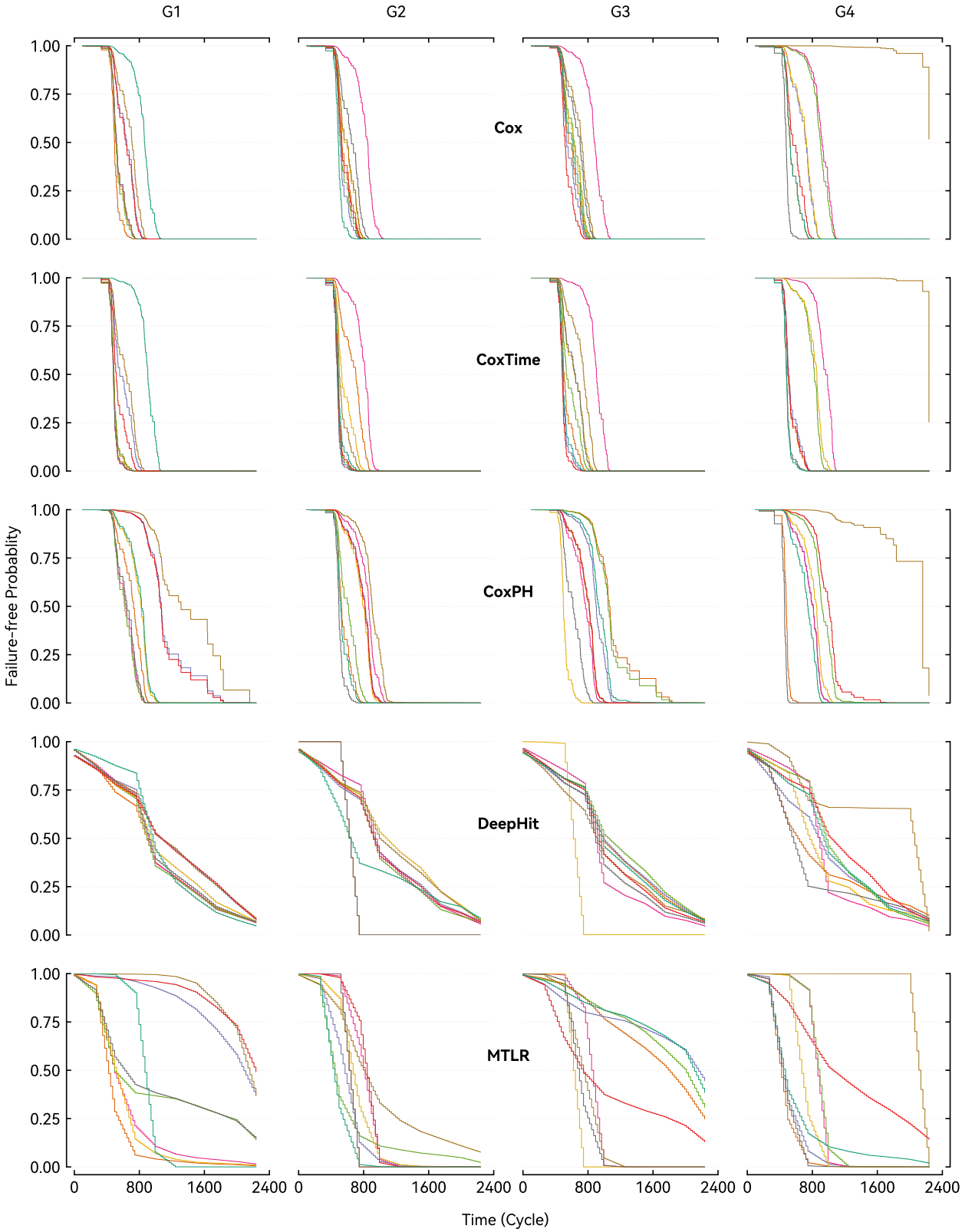

Figure 6: Toyota battery survival curves yielded by the five models for charging.

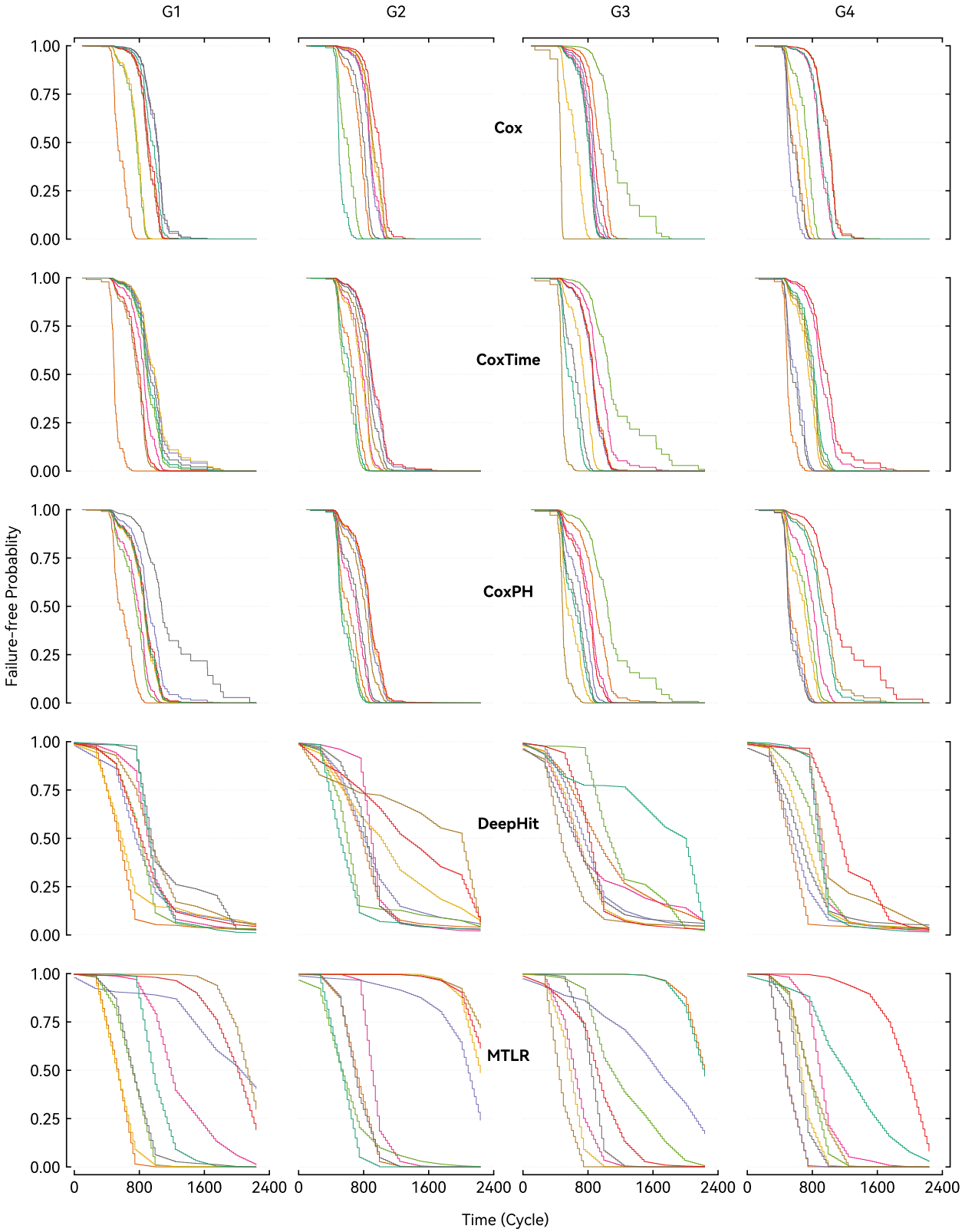

Figure 7: Toyota battery survival curves yielded by the five models for discharging.

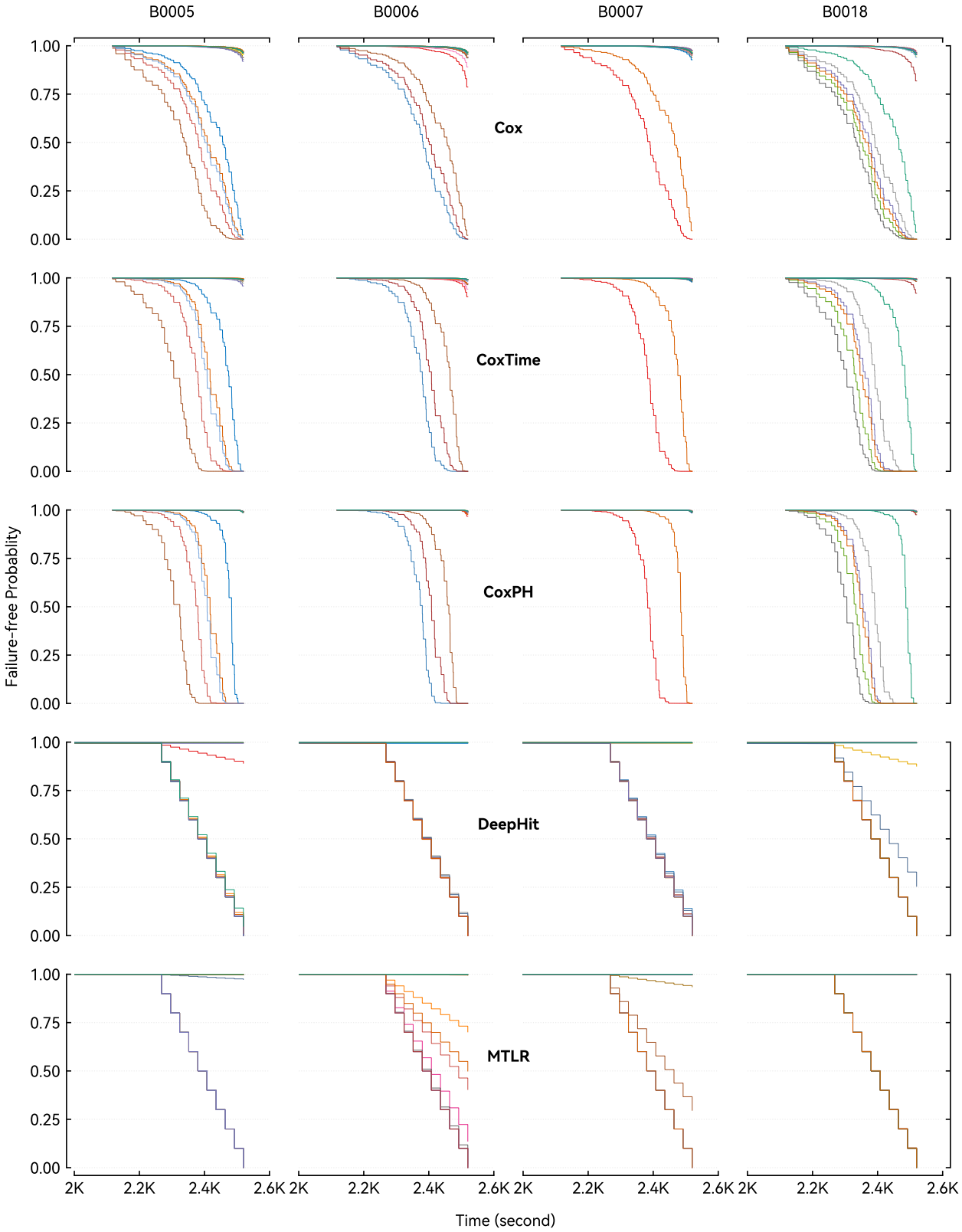

Figure 8: NASA battery survival curves yielded by the five models for discharging.

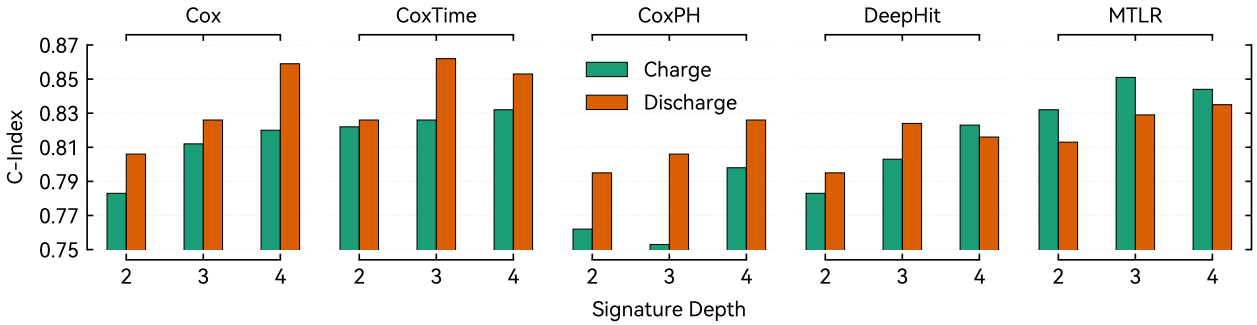

Figure 9: Comparison of models' performance on Toyota data with various transformation depths.

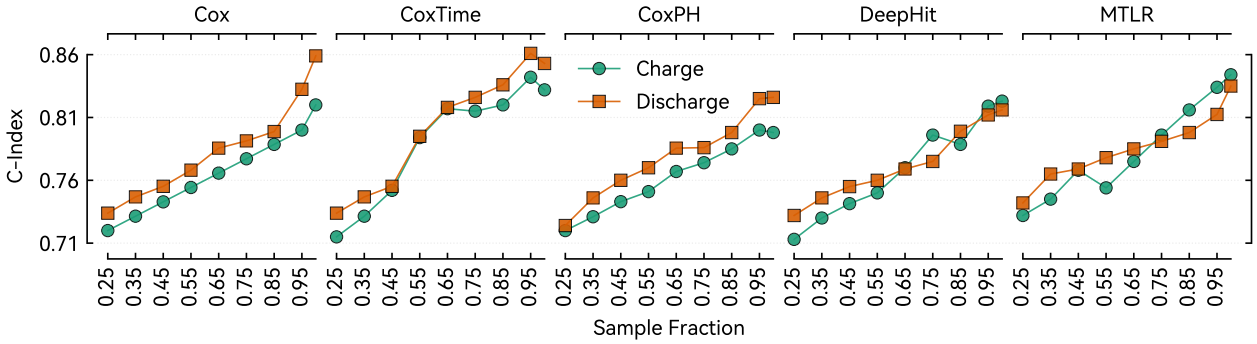

Figure 10: Comparison of models' performance on Toyota data with various splitting fractions.

5 Conclusions

In this study, we proposed a novel survival analysis-based framework for predicting the RUL of Li-ion batteries. The key contributions of this work include the adoption of deep learning techniques for survival analysis, the evaluation of multiple survival models, and the assessment of their generalizability across different signature steps and data splitting proportions. We demonstrated that survival models, particularly DeepHit and MTLR, outperform traditional models such as the Cox Proportional Hazards model in terms of both ranking accuracy and prediction precision. The MTLR model showed excellent performance, achieving the highest C-index and lowest IBS, which indicates its strong generalization ability and robustness in real-world scenarios. Our findings highlight the potential of survival analysis in addressing the challenges of RUL prediction for lithium-ion batteries, especially in dynamic and data-scarce environments. The integration of survival models with advanced feature extraction techniques can significantly improve the accuracy and efficiency of RUL predictions, ultimately supporting the optimization of battery management systems and predictive maintenance strategies. In future work, we plan to explore additional data sources and refine our model further, incorporating more sophisticated feature engineering techniques and real-time battery monitoring data. We also aim to extend our research to other types of batteries used in various applications, such as electric vehicles and renewable energy storage systems.

References

Mohamed Ahwiadi and Wilson Wang. Battery health monitoring and remaining useful life prediction techniques: A review of technologies. *Batteries*, 11(1):31, 2025.

Maher Al-Greer, Imran Bashir, et al. Physics-based model informed smooth particle filter for remaining useful life prediction of lithium-ion battery. *Measurement*, 214:112838, 2023.

Chong Chen, Ying Liu, Shixuan Wang, Xianfang Sun, Carla Di Cairano-Gilfedder, Scott Titmus, and Aris A Syntetos. Predictive maintenance using Cox proportional hazard deep learning. *Advanced Engineering Informatics*, 44:101054, 2020.

Ilya Chevyrev and Andrey Kormilitzin. A primer on the signature method in machine learning, 2025. URL https://arxiv.org/abs/1603.03788.

David Roxbee Cox. Partial likelihood. *Biometrika*, 62(2):269–276, 1975.

Wujin Deng, Yan Gao, Jianxue Chen, Aleksey Kudreyko, Carlo Cattani, Enrico Zio, and Wanqing Song. Multi-fractal Weibull adaptive model for the remaining useful life prediction of electric vehicle lithium batteries. *Entropy*, 25(4):646, 2023.

Bin Duan, Qi Zhang, Fei Geng, and Chenghui Zhang. Remaining useful life prediction of lithium-ion battery based on extended Kalman particle filter. *International Journal of Energy Research*, 44(3):1724–1734, 2020.

Xiaosong Hu, Le Xu, Xianke Lin, and Michael Pecht. Battery lifetime prognostics. *Joule*, 4(2): 310–346, 2020.

Jared L Katzman, Uri Shaham, Alexander Cloninger, Jonathan Bates, Tingting Jiang, and Yuval Kluger. Deepsurv: personalized treatment recommender system using a Cox proportional hazards deep neural network. *BMC Medical Research Methodology*, 18:1–12, 2018.

Mojtaba Kordestani, Mehrdad Saif, Marcos E Orchard, Roozbeh Razavi-Far, and Khashayar Khorasani. Failure prognosis and applications - a survey of recent literature. *IEEE Transactions on Reliability*, 70(2):728–748, 2019.

Håvard Kvamme, Ørnulf Borgan, and Ida Scheel. Time-to-event prediction with neural networks and Cox regression. *Journal of Machine Learning Research (JMLR)*, 20(129):1–30, 2019.

Changhee Lee, William R Zame, Jinsung Yoon, and Mihaela van der Schaar. DeepHit: A deep learning approach to survival analysis with competing risks. *AAAI Conference on Artificial Intelligence (AAAI)*, 32(1):2314–2321, 2018.

De Z Li, Wilson Wang, and Fathy Ismail. A mutated particle filter technique for system state estimation and battery life prediction. *IEEE Transactions on Instrumentation and Measurement*, 63(8):2034–2043, 2014.

Huiqin Li, Zhengxin Zhang, Tianmei Li, and Xiaosheng Si. A review on physics-informed data-driven remaining useful life prediction: Challenges and opportunities. *Mechanical Systems and Signal Processing*, 209:111120, 2024.

Christian Marius Lillelund, Fernando Pannullo, Morten Opprud Jakobsen, Manuel Morante, and Christian Fischer Pedersen. RULSurv: A probabilistic survival-based method for early censoring-

aware prediction of remaining useful life in ball bearings, 2025. URL https://arxiv.org/abs/2405.01614.

Tianjiao Lin, Liuyang Song, Lingli Cui, and Huaqing Wang. Advancing RUL prediction in mechanical systems: A hybrid deep learning approach utilizing non-full lifecycle data. *Advanced Engineering Informatics*, 61:102524, 2024.

Jian Liu and Ziqiang Chen. Remaining useful life prediction of lithium-ion batteries based on health indicator and gaussian process regression model. *IEEE Access*, pages 39474–39484, 2019.

Baohua Mo, Jingsong Yu, Diyin Tang, and Hao Liu. A remaining useful life prediction approach for lithium-ion batteries using Kalman filter and an improved particle filter. In *IEEE International Conference on Prognostics and Health Management (ICPHM)*, pages 1–5, 2016.

Ahmed Ragab, Mohamed-Salah Ouali, Soumaya Yacout, and Hany Osman. Remaining useful life prediction using prognostic methodology based on logical analysis of data and Kaplan-Meier estimation. *Journal of Intelligent Manufacturing*, 27:943–958, 2016.

Yi Ren, Ting Tang, Quan Xia, Kun Zhang, Jun Tian, Daozhong Hu, Dezhen Yang, Bo Sun, Qiang Feng, and Cheng Qian. A data and physical model joint driven method for lithium-ion battery remaining useful life prediction under complex dynamic conditions. *Journal of Energy Storage*, 79:110065, 2024.

MS Reza, M Mannan, M Mansor, Pin Jern Ker, TM Indra Mahlia, and MA Hannan. Recent advancement of remaining useful life prediction of lithium-ion battery in electric vehicle applications: A review of modelling mechanisms, network configurations, factors, and outstanding issues. *Energy Reports*, 11:4824–4848, 2024.

Jiang Xing, Huilin Zhang, and Jianping Zhang. Remaining useful life prediction of lithium batteries based on principal component analysis and improved Gaussian process regression. *International Journal of Electrochemical Science*, 18(4):100048, 2023.

Chun-Nam Yu, Russell Greiner, Hsiu-Chin Lin, and Vickie Baracos. Learning patient-specific cancer survival distributions as a sequence of dependent regressors. *Advances in Neural Information Processing Systems (NIPS)*, 24, 2011.

Hengshan Zhang, Di Wu, Zhongmin Wang, Yanping Chen, and Jiaxuan Xu. Remaining useful life prediction of lithium battery via neural network ensemble. In *International Conference on Intelligent Systems and Knowledge Engineering (ISKE)*, pages 392–397, 2021.

Jianfei Zhang, Lifei Chen, Yanfang Ye, Gongde Guo, Rongbo Chen, Alain Vanasse, and Shengrui Wang. Survival neural networks for time-to-event prediction in longitudinal study. *Knowledge and Information Systems (KAIS)*, 62:3727–3751, 2020.

Brahim Zraibi, Chafik Okar, Hicham Chaoui, and Mohamed Mansouri. Remaining useful life assessment for lithium-ion batteries using CNN-LSTM-DNN hybrid method. *IEEE Transactions on Vehicular Technology*, 70(5):4252–4261, 2021.